Finite prism approach for stability analysis of laminated glass fins

Luiz A. T. Mororó[1], Evandro Parente Jr.[2], Raimundo C. Melo Neto[3]

[1]*Instituto Federal do Ceará, Campus Fortaleza*
Av. Treze de Maio, 2081 - Benfica, 60040-531, Fortaleza/CE-Brazil
luiz.mororo@ifce.edu.br
[2]*Laboratório de Mecânica Computacional e Visualização, Departamento de Engenharia Estrutural e Construção Civil, Universidade Federal do Ceará*
Campus do Pici, Bloco 728, 60440-900, Fortaleza/CE-Brazil
evandro@ufc.br
[3]*RCM - Estruturas Metálicas LTDA*
Av. Desembargador Moreira, 2020, 60170-002, Fortaleza, Ceará, Brazil
rcm@rcmproj.com.br

Abstract. Laminated glass (LG) can be obtained by bonding two or more pieces of glass by means of polymeric interlayers. LG fins are well-known slender elements that are susceptible to flexural buckling under compressive loads, requiring specific calculation methods and verification procedures in order to guarantee appropriate and safe structural performance. This problem has been modeled using Finite Element Method, usually, using shell elements, or analytical models. This work presents an efficient and accurate approach to evaluate elastic critical buckling loads of LG columns applying Finite Prism Method. The accuracy of the proposed approach is assessed comparing the results obtained using solid finite element and analytical models for fully monolithic glass columns, as well as LG columns composed by multiple glass layers.

Keywords: Laminated glass, Finite Prism Method, Buckling

1 Introduction

The use of laminated glass (LG) as a structural material for load-bearing components within buildings has been growing over the last decades. LG can be obtained by bonding two or more pieces of glass by means of polymeric interlayers (*e.g.*, poly vinyl butiral and ionoplast interlayers). This building process gives LG elements a huge advantage over the same ones made of fully monolithic glass with respect to safety, since after breakage fragments usually remain attached to the interlayer, reducing the risk of injuries. As LG columns (also called *fins*) usually present a high slenderness, they are susceptible to flexural and lateral torsional buckling instabilities under compressive loads [1], requiring specific calculation methods and verification procedures in order to guarantee appropriate and safe structural performance [2, 3].

The prediction of the elastic critical buckling loads of LG fins have been determined using Finite Element Method (FEM), generally using shell elements, or analytical models. Usually, such approaches make use of the concept of effective thickness, in which the thickness of a monolithic element with equivalent bending properties in terms of stress and deflection is employed [2, 4–7]. However, the effective thickness approach is either difficult to apply or inaccurate [7].

Despite being a versatile tool, FEM-based models can be very demanding in terms of computational cost, due to the large number of degrees of freedom required to obtain accurate response, and model generation, *i.e.*, defining geometry, boundary and load conditions. On the other hand, analytical models, such as the one proposed by Galuppi and Royer-Carfagni [5], are very efficient, but it is difficult to apply to complex boundary and load conditions, and cross sections consisting of glass panels with different thickness.

In this context, another option would be the use of Finite Prism Method (FPM). The FPM can be considered a particular case of FEM. The main difference between them relies on the fact that FEM makes use of polynomial shape functions in all directions, while the FPM uses a sum of product of polynomial shape functions on the cross-section domain and trigonometric shape functions in the longitudinal direction, which must satisfy essential boundary condition [8]. With this shape function separation, mesh discretization is only required on the

cross section, reducing drastically the computational cost of the analysis and simplifying model generation. Besides, the adopted FPM approach does not make any kinematic assumptions, for instance, Navier-Euler-Kirchhoff hypotheses, as found in many structural formulations.

These FPM features might be very beneficial for multiparametric problems, such as optimization and reliability analyses, where it is usually necessary to assess the evolution of mechanical responses as a function of input parameter variations. Nevertheless, whatever the problem used, it is important to employ a tool that is accurate and robust, and maintains computational cost as low as possible.

In this spirit, this work presents an efficient and accurate approach to evaluate elastic critical buckling loads of LG fins applying FPM. The FPM formulation presented in this study follows the ones by Cheung and Chan [9] and Cheung and Tham [8]; more specifically, we follow the version by Nguyen *et al.* [10]. It is important to emphasize that the application of FPM to such problem, to the best of the authors' knowledge, has not been reported yet. The accuracy of the proposed approach is assessed comparing the results obtained using solid finite element and analytical models for fully monolithic glass fins, as well as LG fins composed by multiple glass layers.

2 Finite prism formulation for elastic buckling analysis

In this section, the main matrices (global stiffness matrix and global geometric stiffness matrix) to perform a linear buckling analyses of LG fins are outlined. In this study, a straight LG fin is discretized with n prism elements on its rectangular cross section whose lengths are set the same of that of the fin, as schematically depicted in Fig. 1.

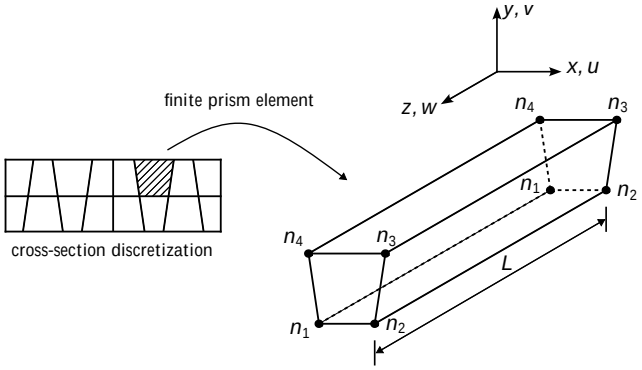

Figure 1. Typical cross-section discretization and finite prism element of four nodes (n_i).

The cross section of the fin is meshed with four-node isoparametric elements while spatial discretization is not employed in its longitudinal direction. The displacement field, described by the components u, v, and w, at any arbitrary point within a prism is approximated by interpolating its nodal displacements with shape functions obtained by the sum of the product of bilinear shape functions on the cross section and trigonometric functions in the longitudinal direction of the fin raging from 1 to m longitudinal terms:

$$\mathbf{u} = \mathbf{N}\mathbf{d} = \sum_{p=1}^{m} \mathbf{N}_p \mathbf{d}_p; \tag{1}$$

where $\mathbf{u}$ is the vector containing u, v, and w, and $\mathbf{d}$ is the vector in which its elements are assembled from the vector $\mathbf{d}_p$ that contains the degrees of freedom (DOF) $\{u_1\ v_1\ w_1\ u_2\ v_2 \quad w_4\}^{\mathrm{T}}_p$ attached to each longitudinal term p (see Fig. 1), whereas the shape function matrix $\mathbf{N}$ can be assembled from the building block matrix $\mathbf{N}_p$ of a single longitudinal term p:

$$\mathbf{N}_p = \begin{bmatrix} \mathbf{N}_1 & \mathbf{N}_2 & \mathbf{N}_3 & \mathbf{N}_4 \end{bmatrix}; \quad \text{where} \quad N_i = \begin{bmatrix} N_i Z_p & 0 & 0 \\ 0 & N_i Z_p & 0 \\ 0 & 0 & N_i Z_p^{\theta} \end{bmatrix}; \tag{2}$$

with i ranging from 1 to 4 (*i.e.*, the number of nodes of a single element on the cross section), N_i being bilinear shape functions obtained by Lagrange's interpolation formula in two directions (x and y), and Z_p and its derivative with respect z, Z_p^{θ}, are trigonometric functions that satisfies specific boundary conditions. In this study, only simply supported ends are considered:

$$Z_p = \sin \frac{p\ z}{L}; \tag{3}$$

where L is the length of a fin. Observe that Z_p is used for u and v, and Z_p^{θ} for w. This comes from the fact that each prism is treated as a beam under small strain/displacement, such that the axial displacement is determined using the slope of the deflection [8, 10].

In applying the approach used in this study, it is also necessary to define the relationship between the strain and displacement fields. Here, the Green-Lagrangian strain tensor is used:

$$"_{ij} = \frac{1}{2}\left(\frac{@u_i}{@x_j} + \frac{@u_j}{@x_i}\right) + \frac{1}{2}\frac{@u_k}{@x_i}\frac{@u_k}{@x_j}; \quad \text{with} \quad i; j; k = 1; 2; 3: \tag{4}$$

Observe that index notation has been employed in the equation above. Also, note that Voigt notation can be applied by using the relation $(x_1; x_2; x_3) = (x; y; z)$, $(u_1; u_2; u_3) = (u; v; w)$. Adopting the hypothesis of small strains, the quadratic terms in eq. (4) can be dropped. This results in the classic form of the small strain vector, ε, which can be written in a matrix-vector relation as:

$$\varepsilon = \mathbf{B}\mathbf{d} = \sum_{p=1}^{m} \mathbf{B}_p \mathbf{d}_p; \tag{5}$$

where $\mathbf{B}$ is the so-called strain-displacement matrix. By the definitions in eqs. (2) and (4), the matrix $\mathbf{B}$ can be assembled from the following building block matrix $\mathbf{B}_p$ that corresponds to a single longitudinal term p:

$$\mathbf{B}_p = \begin{bmatrix} \mathbf{B}_1 & \mathbf{B}_2 & \mathbf{B}_3 & \mathbf{B}_4 \end{bmatrix}; \quad \text{in which} \quad \mathbf{B}_i = \begin{bmatrix} \frac{@N_i}{@x} Z_p & 0 & 0 \\ 0 & \frac{@N_i}{@y} Z_p & 0 \\ 0 & 0 & N_i Z_p^{\theta\theta} \\ \frac{@N_i}{@y} Z_p & \frac{@N_i}{@x} Z_p & 0 \\ 0 & N_i Z_p^{\theta} & \frac{@N_i}{@y} Z_p^{\theta} \\ N_i Z_p^{\theta} & 0 & \frac{@N_i}{@x} Z_p^{\theta} \end{bmatrix}; \quad \text{with} \quad i = 1; 2; 3; 4: \tag{6}$$

The elastic stiffness matrix, $\mathbf{k}_{\mathrm{e}}$, can be derived by using the internal strain energy, U:

$$U = \frac{1}{2}\int_V \varepsilon^{\mathrm{T}}\boldsymbol{\sigma}\,\mathrm{d}V = \frac{1}{2}\sum_{p=1}^{m}\sum_{q=1}^{m} \mathbf{d}_p^{\mathrm{T}}\left(\int_V \mathbf{B}_p^{\mathrm{T}}\mathbf{D}\mathbf{B}_q\,\mathrm{d}V\right)\mathbf{d}_q = \frac{1}{2}\sum_{p=1}^{m}\sum_{q=1}^{m} \mathbf{d}_p^{\mathrm{T}}\mathbf{k}_{\mathrm{e}}^{pq}\mathbf{d}_q = \frac{1}{2}\mathbf{d}^{\mathrm{T}}\mathbf{k}_{\mathrm{e}}\mathbf{d}; \tag{7}$$

where V is the volume of a prism, and $\mathbf{k}_{\mathrm{e}}^{pq}$ is the elastic stiffness matrix related to strains and stresses that comes from Z_p and Z_q, respectively. Two points of extra attention exist in the mathematical development above. First, the constitutive matrix $\mathbf{D}$ that relates stresses and strains, *i.e.*, $\boldsymbol{\sigma} = \mathbf{D}\varepsilon$, according to Hooke's law for three-dimensional problems has been used in the second step. Second, only the linear terms of eq. (4), *i.e.*, eq. (5), has been also used in the second step above.

The geometric stiffness matrix for the elastic buckling analysis can be derived from an additional work created by nonlinear terms only presented in the longitudinal strain component, *i.e.*, $"_z$ (see eq. (4)), of buckling displacements. Therefore, considering only axial buckling problem, the additional work W can be expressed as:

$$\begin{aligned} W &= \frac{1}{2}\int_V {}^{-}{}_z\left[\left(\frac{@u}{@z}\right)^2 + \left(\frac{@v}{@z}\right)^2 + \left(\frac{@w}{@z}\right)^2\right]\mathrm{d}V = \frac{1}{2}\sum_{p=1}^{m}\sum_{q=1}^{m}\mathbf{d}_p^{\mathrm{T}}\left(\int_V {}^{-}{}_z\mathbf{G}_p^{\mathrm{T}}\mathbf{G}_q\,\mathrm{d}V\right)\mathbf{d}_q \\ &= \frac{1}{2}\sum_{p=1}^{m}\sum_{q=1}^{m}\mathbf{d}_p^{\mathrm{T}}\mathbf{k}_{\mathrm{g}}^{pq}\mathbf{d}_q = \frac{1}{2}\mathbf{d}^{\mathrm{T}}\mathbf{k}_{\mathrm{g}}\mathbf{d} \end{aligned}; \tag{8}$$

where ${}^{-}{}_z$ is the axial stress given by an external force, $\mathbf{k}_{\mathrm{g}}^{pq}$ is the element geometric stiffness matrix related to Z_p and Z_q (similarly to the element stiffness matrix in eq. (7)), and $\mathbf{G}_p$ (consequently, $\mathbf{G}_q$) is the matrix containing the partial derivatives of the shape functions which can be obtained as [10]:

$$\mathbf{G}_p = \begin{bmatrix} \mathbf{G}_1 & \mathbf{G}_2 & \mathbf{G}_3 & \mathbf{G}_4 \end{bmatrix}; \quad \text{where} \quad \mathbf{G}_i = \begin{bmatrix} N_i Z_p^{\theta} & 0 & 0 \\ 0 & N_i Z_p^{\theta} & 0 \\ 0 & 0 & N_i Z_p^{\theta\theta} \end{bmatrix} \quad \text{with} \quad i = 1; 2; 3; 4: \tag{9}$$

Remarks can be made related to the integrations in eqs. (7) and (8) to obtain $\mathbf{k}_e$ and $\mathbf{k}_g$, respectively. In this work, such volumetric integrations are carried out in two steps. Firstly, we integrate with respect to z, in which quantities depending on x and y are treated as constants during this integration step, and it is usually carried out analytically leading to the following useful expression [8–10]:

$$I_1 = \int_0^L Z_p Z_q \, dz = \frac{L}{2}; \quad I_2 = \int_0^L Z_p^{00} Z_q \, dz = \frac{{}^2p^2}{2L}; \quad I_3 = \int_0^L Z_p Z_q^{00} \, dz = \frac{{}^2p^2}{2L};$$
$$I_4 = \int_0^L Z_p^{00} Z_q^{00} \, dz = \frac{{}^4p^4}{2L^3}; \quad I_5 = \int_0^L Z_p^{0} Z_q^{0} \, dz = \frac{{}^2p^2}{2L} \tag{10}$$

if $p = q$, otherwise, $I_1 = I_2 = I_3 = I_4 = I_5 = 0$. Note that these results are for the case of simply supported fins. Finally, numerical integration scheme, such as Gaussian quadrature, is employed to integrate over the cross section.

The linearized buckling analysis carried out in this work consists in solving the generalized eigenproblem defined as:

$$(\mathbf{K}_e + \mathbf{K}_g)\,\mathbf{\Phi} = \mathbf{0}; \tag{11}$$

where $\mathbf{K}_e$ is the global stiffness matrix assembled through element stiffness matrices (see eq. (7)), $\mathbf{K}_g$ is the global geometric stiffness matrix assembled through element geometric stiffness matrices (see eq. (8)) for the reference load, are the eigenvalues associated with the buckling load factors, and $\mathbf{\Phi}$ are the buckling modes.

3 Numerical examples

The numerical examples in this section are inspired by the lateral torsional buckling stability problem following Bedon [3]. The case consists of a simply supported fin whose length is $L = 4000\,\text{mm}$ and height is equal to $h = 450\,\text{mm}$, as schematically illustrated in Fig. 2. Young's modulus and Poisson's ratio of the glass panels are, respectively, $E_g = 70\,000\,\text{MPa}$ and $_g = 0{:}22$. Two types of cross sections are investigated, one with two (CS2) and other one with three glass panels (CS3). For both configurations, the thickness of each glass panel and interlayer are, respectively, $t_g = 12\,\text{mm}$ and $t_{int} = 1{:}52\,\text{mm}$. All the simulations with FPM are performed with only one longitudinal term $m = 1$ (see eq. (1)).

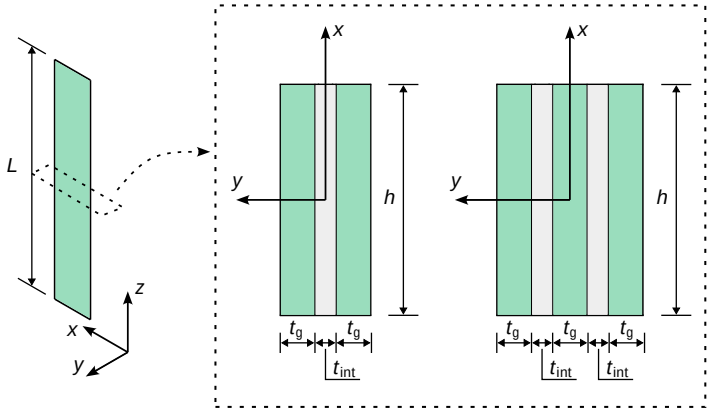

Figure 2. Geometry of the LG fins and cross sections with two (CS2) and three glass panels (CS3).

3.1 Monolithic fins

In this first example, a convergence study is conducted for a monolithic fin whose cross section has the same dimensions as CS2, *i.e.*, $24{:}52\,(2t_g + t_{int})$ $450\,\text{mm}$. The aim of this example is to demonstrate the ability of the proposed approach to converge to the analytical solutions obtained from Euler's formulas for critical axial buckling (N_{cr}) load and critical buckling moment (M_{cr}) [11]. The boundary conditions are illustrated in Fig. 3.

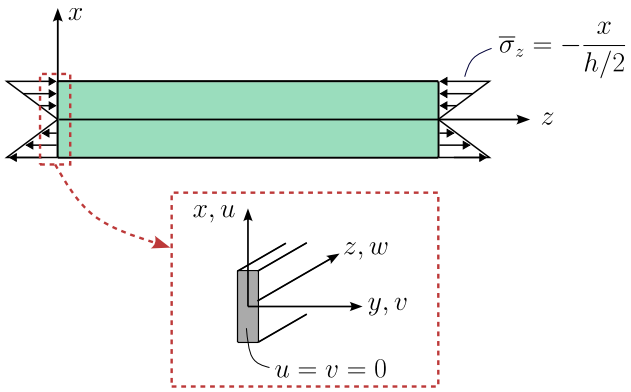

Figure 3. Boundary conditions.

The cross section is discretized with three layers of element through height, while the number of elements is varied through width, as schematically exemplified in Fig. 1. Fig. 4a shows the relative error between FPM and analytical solutions for N_{cr} and M_{cr}, indicating a good convergence rate and monotonic behavior, with the FPM critical load decreasing with mesh refinement. Fig. 4b shows the lateral torsional buckling mode for M_{cr} obtained with the finite prism approach.

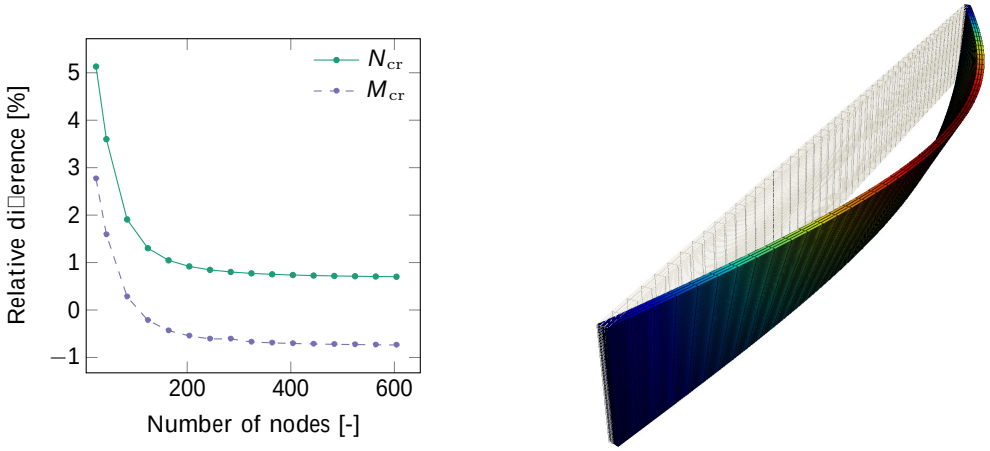

(a) Convergence study.

(b) Lateral torsional buckling mode.

Figure 4. Monolithic fin.

3.2 Laminated glass fins

In this final example, the proposed FPM formulation is applied for the case of the two LG fin configurations. Boundary and load conditions are the same, as detailed previously. In order to simulate temperature and load dependencies of interlayers, Young's modulus of the interlayers are varied [2, 4]. Tables 1 and 2 show the results as well as comparisons between FPM and FEM. For FEM results, we model all the LG fins with 20-node brick-like element with reduced integration. For both configurations CS2 and CS3, only one element is applied in each ply (glass and interlayer). The approximate global size of each finite solid element is 50 mm, which yields 12997 nodes for CS2 and 23413 nodes for CS3. The same discretization scheme is used for FPM on the cross sections.

Table 1. Results for CS2.

E_{int} (MPa)	N_{cr}			M_{cr}		
	FEM (kN)	FPM (kN)	Diff. (%)	FEM (MN m)	FPM (MN m)	Diff. (%)
1	16.057	15.750	-1.91	16.326	15.982	-2.11
5	22.948	23.198	1.09	21.762	21.706	-0.26
10	24.746	25.006	1.05	24.811	24.752	-0.24
100	26.751	26.996	0.92	36.634	36.459	-0.48
200	26.896	27.122	0.84	39.018	38.818	-0.51
500	26.997	27.200	0.75	41.074	40.849	-0.55

Table 2. Results for CS3.

E_{int} (MPa)	N_{cr}			M_{cr}		
	FEM (kN)	FPM (kN)	Diff. (%)	FEM (MN m)	FPM (MN m)	Diff. (%)
1	33.919	34.425	1.49	29.824	29.769	-0.18
5	66.435	66.967	0.80	48.345	48.088	-0.53
10	77.433	77.970	0.69	59.177	58.829	-0.59
100	91.642	92.185	0.59	109.572	108.857	-0.65
200	92.610	93.159	0.59	122.781	121.982	-0.65
500	93.212	93.772	0.60	134.830	133.971	-0.64

From Tables 1 and 2, we can observe an excellent agreement between the numerical models for both CS2 and CS3, in which the maximum absolute difference is 2.11 % for CS2 when M_{cr} is considered (see Table 1). Fig. 5 shows the lateral torsional buckling mode and a close-up detailing the relative displacement (*i.e.*, a zig-zag behavior) of plies for CS3 at a given location of the LG fin obtained with the finite prism approach.

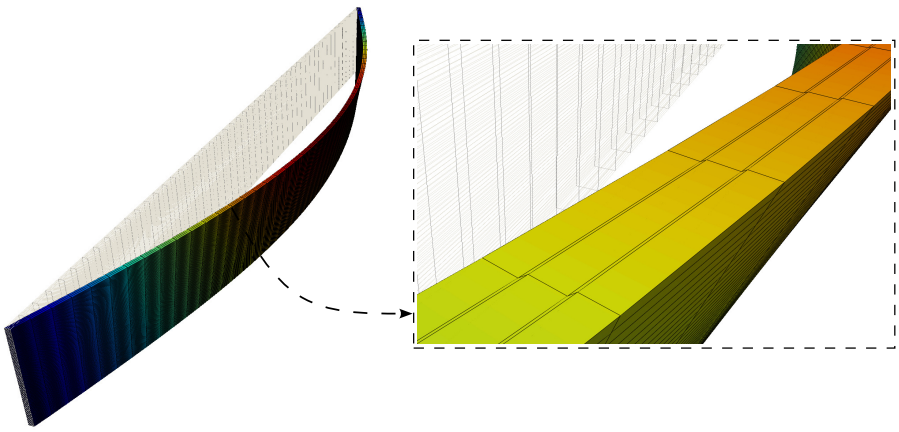

Figure 5. Lateral torsional buckling mode for CS3.

4 Conclusion

This work presented a finite prism framework for the determination of critical buckling loads of simply supported laminated glass fins. On the cross section, four-node elements have been employed, where each node has

three DOFs (displacements) attached to, whereas one single half sine wave has been employed in the longitudinal direction.

In two examples, a successful FPM implementation has been shown. The convergence study show that the finite prism approach presents a good convergence rate with regard to analytical solutions for both N_{cr} and M_{cr} for monolithic fin. The results show that it is possible to apply the FPM to different variations of LG fins. The quality of the results are not influenced by either the number of glass plies and interlayer properties when compared with results obtained from finite solid models. This is a necessary feature in order to use the finite prism approach in multiparametric settings, such as optimization and reliability analyses, in which computational cost might be a real bottleneck.

Acknowledgements. The authors gratefully acknowledge the financial support provided by CNPq (Conselho Nacional de Desenvolvimento Científico e Tecnológico).

Authorship statement. The authors hereby confirm that they are the sole liable persons responsible for the authorship of this work, and that all material that has been herein included as part of the present paper is either the property (and authorship) of the authors, or has the permission of the owners to be included here.

References

[1] X. Huang, S. Duan, Q. Liu, J. Nie, and W. Han. Investigation on buckling behavior of laminated glass columns with elastic lateral restraint under axial compression. *Composite Structures*, vol. 279, pp. 114810, 2022.
[2] C. Bedon and C. Amadio. Design buckling curves for glass columns and beams. *Proceedings of the Institution of Civil Engineers - Structures and Buildings*, vol. 168, n. 7, pp. 514–526, 2015.
[3] C. Bedon. Lateral-torsional buckling (ltb) method for the design of glass fins with continuous lateral restraints at the tensioned edge. *Composite Structures*, vol. 266, pp. 113790, 2021.
[4] L. Galuppi and G. F. Royer-Carfagni. Effective thickness of laminated glass beams: New expression via a variational approach. *Engineering Structures*, vol. 38, pp. 53–67, 2012.
[5] L. Galuppi and G. F. Royer-Carfagni. Enhanced effective thickness of multi-layered laminated glass. *Composites Part B: Engineering*, vol. 64, pp. 202–213, 2014.
[6] L. Galuppi and G. F. Royer-Carfagni. Enhanced effective thickness for laminated glass beams and plates under torsion. *Engineering Structures*, vol. 206, pp. 110077, 2020.
[7] G. D'Ambrosio and L. Galuppi. Enhanced effective thickness model for buckling of lg beams with different boundary conditions. *Glass Structures & Engineering*, vol. 5, pp. 205–2010, 2020.
[8] Y. K. Cheung and L. G. Tham. *Finite Strip Method*. Taylor & Francis Group, United States, 1998.
[9] M. Cheung and M. Chan. Three-dimensional finite strip analysis of elastic solids. *Computers & Structures*, vol. 9, n. 6, pp. 629–638, 1978.
[10] H.-D. Nguyen, G.-W. Jang, D.-M. Kim, and Y. Y. Kim. Finite prism method based topology optimization of beam cross section for buckling load maximization. *Structural and Multidisciplinary Optimization*, vol. 57, pp. 55–70, 2018.
[11] T. V. Galambos and A. E. Surovek. *Structural Stability of Steel: Concepts and Applications for Structural Engineers*. John Wiley & Sons, New Jersey, USA, 1 edition, 2008.